Oxygen Reduction Reaction Promotes Li^+ Desorption from Cathode Surface in Li-O_2 Batteries

Marta Haro*, Nuria Vicente, and Germà Garcia-Belmonte*

Photovoltaic and Optoelectronic Devices Group, Departament de Física, UniversitatJaume I, 12071 Castelló, Spain

Correspondign authors Email: mharo@uji.es,garciag@uji.es

Abstract

Li-O_2 batteries are claimed to be one of the future energy storage technologies since it could provide a specific energy as high as 3500Wh kg^{-1}. A great number of scientific and technological challenges should be solved firstly to transform Li-O_2 battery from a promise to real practical devices. Proposed mechanisms for oxygen reduction assume a reservoir of solved Li^+ ions in the electrolyte. However, the role that adsorbed Li^+ on the electrode surface might have on the overall oxygen reduction reaction (ORR) has not deserved much attention. Adsorbed Li^+ consumption is monitored here providing a new perspective on the design of Li-O_2 batteries. The discharge process of a Li-air battery has been analyzed by impedance spectroscopy identifying kinetically-separated steps. Adsorbed Li^+ is inferred from extended electrochemical double layer capacitance, which depends on the carbon matrix surface area. The presence of O_2 drastically reduces the amount of adsorbed Li^+ signaling the kinetic competition between Li^+ surface adsorption and its consumption only for potentials corresponding to the oxygen reduction reaction. Noticeably double layer capacitance remains unaltered after cycling. This fact suggests that the ORR products (Li_2O_2 and Li_2CO_3) are not covering the

internal electrode surface, but deposited on the outer electrode-contact interface, hindering thereby the subsequent reaction. Current results show new insights into the discharge mechanism of Li-O_2batteries and reveal the evidence of Li^+ desorption from the C surface when the oxygen reduction reaction starts.

Published

Advanced Energy Materials **2** (2015) 1500369, DOI:10.1002/admi.201500369

1. Introduction

In an increasingly energy-dependent society, the need for renewable energy sources together to its storage is paramount to maintain current society paradigm in a sustainable way with the environment. Albeit Li batteries (LIBs) have invaded the electronic market, their energy densities are usually limited below 250 Wh kg^{-1}[1]. This limitation is mainly originated by the mechanisms through which the chemical energy is stored in the present commercial LIBs that is based on the reversible reaction of the electrode materials with Li^+ ions by means of intercalation mechanisms. Therefore, approaches based on new chemistry are necessary to increase the energy density in batteries, such as Li-S and Li-O_2, which can provide more than 1000 Wh kg^{-1}[1-2].In particular, Li-O_2 batteries have received a great deal of attention as they can deliver the highest energy density among any other type of batteries. Li^+ ions and O_2 directly react with each other in the absence of any heavy transition metals or crystal framework.[3] Nevertheless, Li-O_2 battery technology is in its infancy and many fundamental issues are needed to be addressed before their practical application.

The chemical energy storage in Li-O_2 batteries is based on the oxygen reduction reaction (ORR) during discharge and oxygen evolution reaction (OER) in the charge, $2\ Li^+ + O_2 + 2\ e^- \leftrightarrow Li_2O_2$ (E^o = 2.96 V, with theoretical specific energy of 3500 $Whkg^{-1}$). To date, Li_2O_2 has been identified as the main discharge product by different techniques like Raman spectroscopy [4] and AFM [5]. Li_2O_2 is electronically insulating, very oxidative and insoluble, precipitating onto the electrode what causes the increase of the necessary potential for oxygen evolution reaction (OER) and the oxidation of the carbon electrode and/or electrolyte giving Li_2CO_3,[6] and as consequence the decrease of the cycleability of the Li-O_2 battery. Also, some authors

note that the insulating nature of Li_2O_2 avoids its possible reduction to Li_2O, in this situation, Li-O_2 batteries would provide energy densities as high as 5200 Wh kg^{-1}[7].

It is then noticeable that to fully exploit the capacity of Li-O_2 batteries, the thermodynamic and kinetic mechanisms that govern and limit their functioning must be understood. From the pioneering studies of Abraham et al.[8] on the ORR to date, the oxygen reduction reaction has been widely analyzed in Li-O_2 batteries[9], and several models have been proposed, which have been recently unified by Bruce et al. [10]. Generally, the adsorption of O_2 molecules onto the cathode with one electron interchanged with the electrode is considered as the first step ($O_2 + e^- \leftrightarrow O_2^-$, $E^o = 2.71$ V). This adsorbed O_2^- reacts with Li^+ ions to produce LiO_2adsorbed or as solid dissolved in the electrolyte. Depending on the solvent nature and the chemisorption strength with the cathode different mechanisms have been proposed for the reaction of the adsorbed LiO_2 with Li^+ ions until Li_2O_2 is reached as final product. In all these studies, the ORR starts with the reduction of oxygen in the context of free electrode surface and solved Li^+ ions in the electrolyte. However, the role that adsorbed Li^+ ions on the electrode surface might have on the overall ORR has not deserved much attention. This last contribution was pointed out by Qu et al. [11], although no experimental evidence was provided. The monitoring for the first time of the desorption process of Li^+ ions induced by ORR provides here revealing insights on the cathode surface processes in Li-O_2 batteries.

In this manuscript, Li-O_2 discharge process in different cathodes has been monitored by electrochemical impedance spectroscopy (EIS). This technique has been recently used suggesting that the overpotential during discharge is caused by internal resistance, and is dominated by the charge transport through the deposited Li_2O_2 at the end of discharge.[6, 12] Our study is based on a cathode made by carbon Super P with 30% of

NiOCoO as catalyst in the presence and absence of O_2. Actually, both cathodes (with and without O_2) show the same impedance spectra from 4.0 to 2.7 V, in which extended electrochemical double layer capacitance (EDLC) made up by adsorbed Li^+ is observed. This behavior has been verified on different systems and tested that is dependent on the surface area of the cathode. At lower voltages, the electrode in the presence of O_2 shows a huge capacitance increase at the same time that the EDLC is reducing. This fact evidences the depletion of the adsorbed Li^+ during the ORR. The results show three steps with their characteristic reaction time and resistance in the Li-O_2 discharge: i) interfacial phenomena, ii) extended electrochemical double layer capacitance (EDLC), and iii) chemical capacitance generated by oxygen reduction reaction (ORR Capacitance). This study gives new insights onto the Li-O_2 discharge mechanism provided by impedance spectra, and highlights the key contribution on the overall ORR of adsorbed Li^+ on the electrode surface.

2. Results and discussion

2.1. Electrochemical behavior in the presence and absence of O_2

Figure 1a shows the cyclic voltammetry (CV) of SP@30NiOCoO in the presence of O_2during cycling and in absence of O_2 (third cycle).Without O_2, the CV signal shows some hysteresis (in the order of few mA g_c^{-1}) without any remarkable peak (inset of Fig. 1a). This shape is characteristic of supercapacitors in which the hysteresis is attributed to the extended electrochemical double layer capacitance (EDLC) built by the adsorption of Li^+ ions onto the carbon surface[13]. In the present case, the hysteresis is low because the surface area of the carbon matrix is small (S_{BET}=75 m^2 g^{-1}) compared to the carbon materials used for supercapacitors. The CV changes drastically in the presence of O_2, where a cathodic peak is observed with an onset at 2.9 V and the

maximum at 2.4 V, with the typical shape reported in the literature [4, 14]. The shift of ORR peak from 2.7 V to 2.4 V has been attributed to the EC mechanism, that is, electrochemical reduction ($O_2 + e^- \rightarrow O_2^-$) followed by a chemical step (reaction ofLi^+ with O_2^-) that severely deplete the concentration of O_2^-[4]. With the number of cycles, the cathodic peak reduces conspicuously, and in rather less extension the anodic peak. For this air cathode (of low S_{BET}), the capacity is ca. 500 mAh g_c^{-1} (Figure SI.1). The main species formed in the discharge process is Li_2O_2, which is almost decomposed during charge process, as revealed the XPS spectra (Figure SI.2) that provides molecular percentage of Li in the form Li_2O_2 at 2.4 V and 3.4 V after 3, 5 and 7 cycles (**Table 1**). XPS also shows that, in this case, $Li_2CO_3$is formed once Li_2O_2 (very oxidative species that can react with the C of the electrode and/or the electrolyte) is produced,[6, 15] albeit in little amount. Nevertheless, the decomposition of this residue is low and while Li_2O_2almost disappears during charge process, the residue reduces nearly a half. The evolution of the electrode composition is observed by XPS, where we could observe that Li_2CO_3 is accumulated, as also pointed out by XRD (**Figure 1b**). Before cycling, the electrode shows the peaks ascribed to the mesh substrate and the catalyst, NiOCoO, the same result than the electrode at 3.4 V (before reduction process) after being cycled 3 times. Nevertheless, the characteristic peaks of Li_2O_2 are observed after 5 CV, peaks that disappear after 7 cycles, where the characteristic Li_2CO_3 peaks are clearly observed.

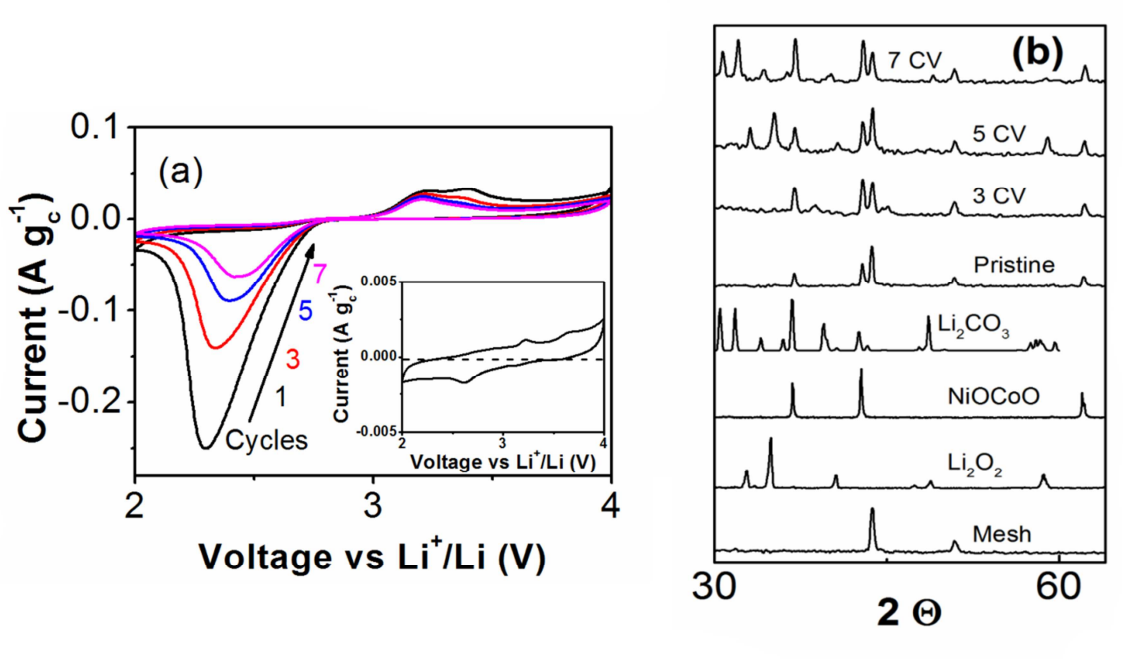

Figure 1a.CV of SP@30NiOCoO in the presence of O_2 along different number of cycles and in the absence of O_2 (inset). Scan rate: 0.1 mV s^{-1}. **b.** XRD patters of air cathode before being cycled (pristine) and after 3, 5 and 7 cycles. The patters of the mesh, Li_2O_2, NiOCoO, and Li_2CO_3 are also shown.

Sample	**Specie (% mol)**	
	Li (Li_2O_2)	**Li (Li_2CO_3)**
3 cycles, 2.4 V	3.6	1.4
3 cycles, 3.4 V	0.3	0.6
5 cycles, 3.4 V	5.6	11.2
7 cycles, 3,4 V	6.9	19.4

Table 1. Molecular percentage of Li in the form of Li_2O_2 and Li_2CO_3 determined by XPS (all data shown in SI) in the sample cycles three, five or seven times at different stop voltage: 2.4 and 3.4 V.

In order to assay the electrode in a representative state during Li-O_2 charge-discharge process, the electrochemical impedance spectroscopy was performed after three CV. The first cycle is discarded because it is not representative of a steady operation, and at

the third cycle residual compounds are negligible, as XPS (Table 1 and Figure SI.2) and XRD (Figure 1.b) data demonstrate. The EIS measurements were carried out potentiostatically at different stages of Li^+ ion insertion at a very low rate to ensure the steady-state condition. **Figure 2** shows three different Nyquist diagrams, representative of the different stages during the discharge process. The low frequencies range of the impedance spectra (below 5 Hz, indicated in Figures 2a and 2b) of both systems give the same Nyquist plot from ca. 3.6 to 2.8 V. At 4.0 V (Figure 2a), the system with O_2 shows lower resistive behavior probably due to the degradation of the carbon cathode and the electrolyte solvent in the presence of O_2, since carbon becomes unstable at voltages above 3.5 V [16]. At 2.6 V (and lower voltages), the Nyquist plot of the cathode in presence of O_2 changes drastically and the arc associated to the low frequency decreases dramatically. A new electrochemical feature is now observed at frequencies lower than 10 mHz (Figure 2f).This process should be related to the limiting step for ORR and O_2diffusion. At high frequencies (above 5 Hz, Figures 2d-f), the Nyquist plots of the battery in absence of O_2 show one arc while there are two smaller arcs in the presence of O_2.

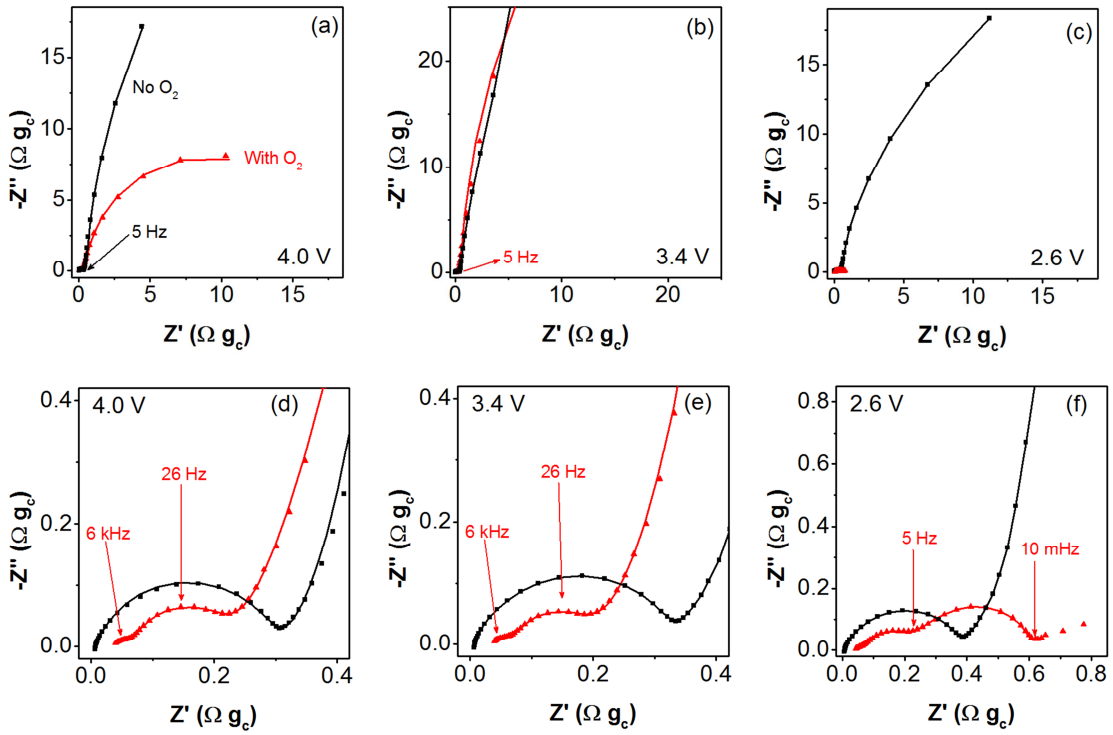

Figure 2. Nyquistplots of SP@30% NiOCoO with and without O_2.The low frequency (< 5 Hz) region of the EIS is observed in graphs a-c, and the figures d-f show an enlargement of the high frequency region. The experimental data are represented by solid symbols and the lines are obtained by the fitting with the equivalent circuit model shown in Figure 4b.

To gain deeper insight on the Li-O_2 discharge kinetics, the impedance data are represented in terms of capacitance ($C = 1/i\omega Z$) in **Figure 3**. In this representation, the real part, C', is related to the electrode charging while the associated resistance caused by kinetic limitations determines the value reached by the imaginary part, C''. As explained elsewhere[17], capacitive representation allows straightforwardly extracting contributing capacitors and, consequently, inferring on charging mechanisms. Each arc in a capacitance plot is assimilated to a *RC* series subcircuit. In the region of low frequencies (below 5 Hz) an arc is observed that closes to ca. 6.5 F g_c^{-1} in the two systems (with and without O_2) within the voltage range 4.0-2.8 V. At lower voltages, a

new arc is observed in the presence of O_2 that is more than two orders of magnitude higher than the previous one, and hides it. At high frequencies (see Figure SI.3), smaller arcs linked to different capacitive features in the multistep discharge process are observed for both systems, although the capacitance in presence of O_2 is larger than in its absence.

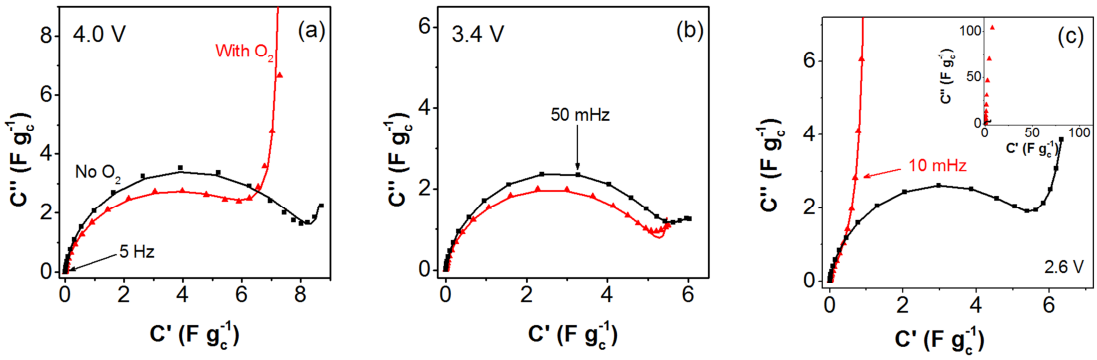

Figure 3. Capacitance plot of SP@30% NiOCoO with and without O_2. The experimental data are represented by solid symbols and the lines are obtained by the fitting with the equivalent circuit model shown in Figure 4.b.

2.2. Electrode mechanisms through equivalent circuits

Figure 4a represents the capacitance spectra, C', vs. characteristic time (inverse of measuring frequency) of the SP@30NiOCoO cathode in the presence (solid lines) and absence (dashed lines) of O_2.The horizontal axis is also represented in frequency scale, inversely than usually drawn, from high to low frequency in order to maintain the same reading direction of the equivalent circuit model. In this representation, a plateau is demonstrative of a capacitive step in the discharge mechanism occurring at a certain frequency range. For electrodes with and without O_2, two plateaus are observed: the first one at intermediate frequencies (ca. 100 Hz) is O_2 dependent, while the second at low frequencies (ca. 0.01 Hz) is O_2 independent only at higher potentials. These two plateaus correspond to the two arcs described in Figures 3 and SI.3. The plateau at low

frequencies is unaltered by the presence of O_2 in all the discharge process until 2.6 V. Noticeably below this potential the presence of O_2induces the capacitance decreasing by one order of magnitude showing a plateau that ends at 10 mHz. At lower frequencies the capacitance further increases in relation with the diffusion and reaction process discussed in Figure 2.f.

By observing Figure 4a one can distinguish three steps in the discharge process, which are marked with squares and represented in the different subcircuits of the equivalent circuit model shown in Figure 4b. The fitting of the proposed equivalent circuit model is represented in Figures 2 and 3 with solid lines. The observed steps during discharge are:

i) Interfacial phenomena (high frequency: >5 Hz) that is O_2dependent. In the presence of O_2 two arcs are observed in the Nyquist plot, which are represented by two resistances (R_{i1} and R_{i2}) in parallel with two capacitances (C_{i1} and C_{i2}). In the absence of O_2, only one arc is observed that is equivalent to a resistance (R_i) in parallel to the capacitance (C_i).

ii) Extended electrochemical double layer capacitance (EDLC) (intermediate frequency: 10 mHz<f < 5 Hz) that is O_2 independent at high potentials. This mechanism is connected to the Li^+ adsorption on the internal electrode surface. This capacitance, C_{EDL}, is associated to an arc in the C'' vs C' representation that can be modeled by a series *RC* circuit[17-18]. The associated resistance R_{ads} accounts for the Li^+ transport in the electrolyte within the porous matrix. More details of this subcircuit model are in Supporting Information.

iii) Chemical ORR capacitance (low frequency: < 10 μHz) that only appears in the presence of O_2. When O_2 starts to react (at 2.8 V and below) a new parallel branch to the EDLC is represented in the equivalent circuit model by the

chemical capacitance, C_μ, in series to the associated resistance, R_{ORR}, accounting for the reduction reaction.

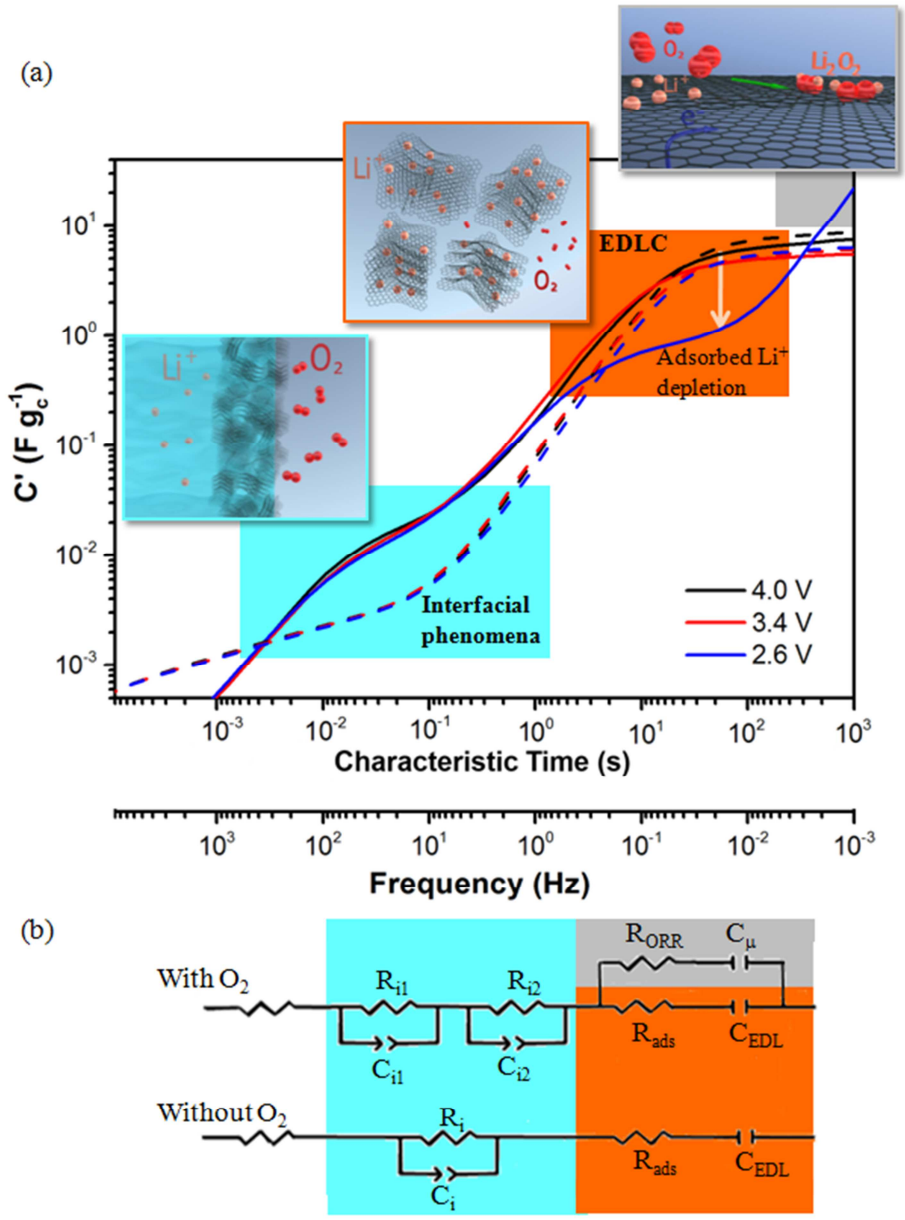

Figure 4.(a)C' vs characteristic time and frequency (in opposite order than usual, from fast to slow electrochemical processes for a more intuitive reading) for SP@30NiOCoO in the presence (solid lines) and absence (dashed lines) of O_2. Inset: Scheme of the three processes of the Li-O_2 discharge mechanism. The ORR is represented on the cathode

surface by a graphitic layer, in which adsorbed Li^+ react with O_2. (b) Equivalent circuit model for the system in the absence and presence of O_2.

2.3. Interfacial phenomena

The electrochemical processes related to the interface are monitored by EIS at high frequencies. In the absence of O_2, a single semi-circle is observed in the Nyquist representation (Figure 2 d-f) that is associated with a semi-circle to the C'' vs C' representation, Figure SI3. This capacitance, C_i, and resistance, R_i, can be associated to the impedance generated at the contact interface between the electrode and the electrolyte solution.[19] In the presence of O_2, two small arcs are distinguished in Figure 2 d-f. One of the arcs can be ascribed to the formation of the isolating layer formed by Li_2O_2 and Li_2CO_3(as XPS and XRD shown) and the other to the impedance at the contact interface, as it has been assigned in the absence of O_2. In any case these resistive elements introduce limitations into the overall charging mechanism.

The fitting values obtained by the equivalent circuit model are represented in **Figure 5**. With the calculated values, we can indicate that C_{i2} and R_{i2} are related to the electrode/electrolyte contact since they are constant independently of the applied voltage. In this assumption, C_{i1} and R_{i1} should be related to the solid electrolyte interface ($Li_2O_2$and Li_2CO_3) formed on the cathode, which explains why the capacitance increases with the oxygen reduction reaction.

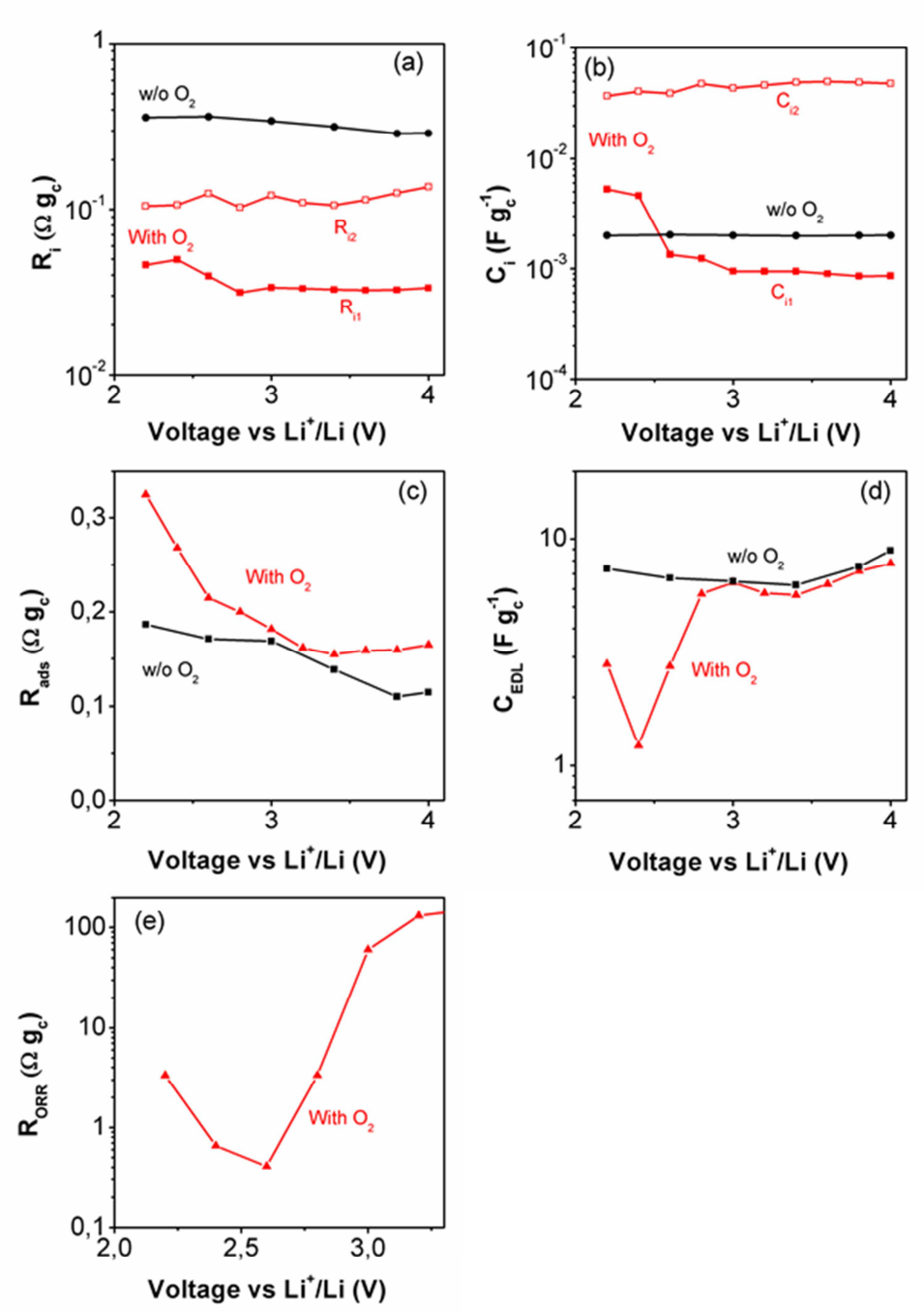

Figure 5. Parameters determined during discharge process by the EIS fitting with the equivalent circuit model shown in Figure 4.b: (a) resistance and (b) capacitance associated to the interface phenomena;(c) resistance, R_{ads}, and (d) capacitance, C_{EDL}, associated to the formation of the electrochemical double layer; (e) parallel resistance, R_{ORR}, which decrease at the applied voltages when the ORR starts.

2.4. Electrochemical double layer capacitance

With the equivalent circuit model (Figure 4b), the main parameters of the Li^+ adsorption step in the discharge process are obtained, **Figure 5**. In the absence of O_2, the capacity is practically constant, 6.5F g_c^{-1}(that corresponds to ca. 8μF cm_c^{-2} considering an area S_{BET}= 75 m^2g^{-1}), independently of the voltage. This value is within the range of reported electrochemical double layer capacitances in supercapacitors based on carbon materials (5-20 μF cm^{-2})[13a]. In this case, the capacitance is in agreement with a lower value obtained with supercapacitors when an organic electrolyte is used compared to aqueous electrolytes[20]. Associated to the charge accumulation by physical electro-adsorption there is a resistance that has been related to the ion transport along the tortuous path of the micro/meso-porosity of the carbon matrix[21]. In the presence of O_2, the EDL capacitance is unaltered at high voltages and noticeably decreases when the ORR starts. This is in accordance with recent capacitance analysis.[12] The resistance of the Li^+ adsorption process consistently increases, showing the kinetic competition between Li^+ adsorption and consumption by ORR at voltages lower than 2.8 V. At the same time, the parallel resistance, R_{ORR}, decreases dramatically (close to three orders of magnitude) giving further support to the idea that the current runs along the parallel branch corresponding to the ORR subcircuit in Figure 4b. At lower voltages than ORR reaction, (i.e. 2.2 V), the capacitance of the EDL starts to increase again signaling a full recovering of the double layer features. We infer that the ORR branch in Figure 4b is kinetically favored at potentials 2.4-2.8 V.

To check the role of species involved in the EDLC formation as a step in the discharge mechanism, other systems have been measured for consistency. The same results have been obtained in the absence of catalyst (Figure SI.4) and the study with carbons of different S_{BET} has revealed that EDLC can be considered only dependent on the carbon

surface area (Figure SI.5). This point is further discussed in the SI since depending on the size of the pores the area can be active or not to the formation of the EDLlike in the case of the supercapacitors.

In order to analyze the effect of cycling on the formation of the electric double layer, the electrochemical impedance spectrum at 3.4 V (during lithiation process) has been registered along several CV cycles. The Nyquist and capacitance plots are represented in **Figure 6** and the obtained fitting parameters in Figure **SI**.6. Surprisingly, no significant differences are observed in the Nyquist plots and the EDL capacitances are practically constant, independently of the cycling number. This result shows that the electrode textural property is not modified with the number of cycles, and Li^+ cations can freely adsorb in the carbon porosity, independently on the formation of Li_2O_2 and Li_2CO_3, which presence is evidenced by XPS and XRD.

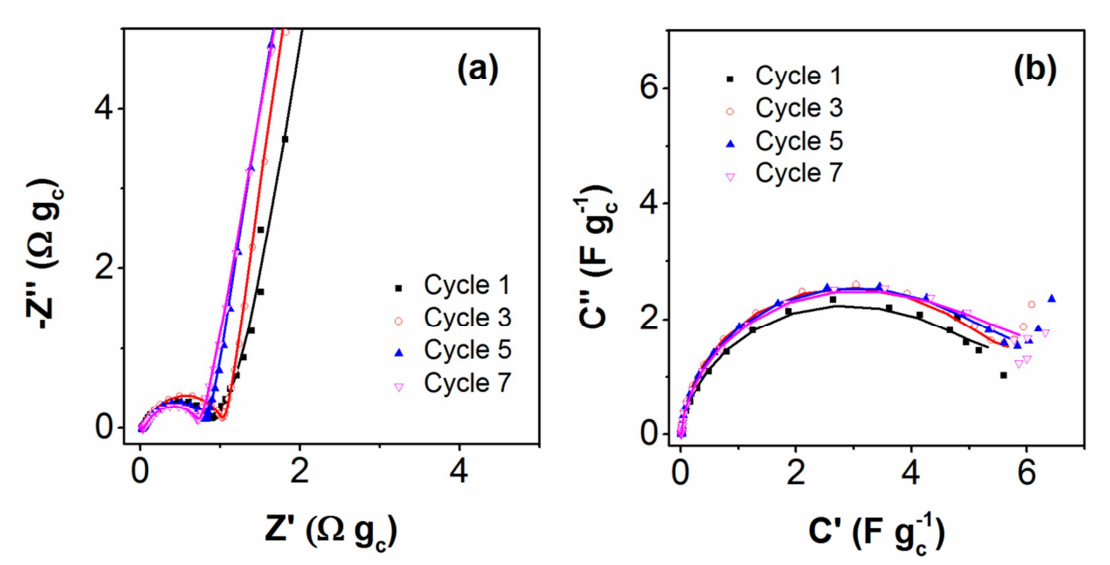

Figure 6. a) Nyquist and b) EDL capacitance plots of the SP@30% NiOCoO air cathode at 3.4 V at different number of CV cycles.

With all the data in mind, the fact that EDL capacitance decreases when ORR starts due to a hiding phenomenon can be discarded since the EDL capacitance remains unaltered

after cycling. If the reaction products (mainly Li_2O_2) partially cover the carbon surface one would expect a reduction of the EDLC with cycling that does not occur at 3.4 V (Fig. 6b). Therefore, the EDLC decrease with ORR should be associated to Li^+ desorption, which can be either caused by: i) displacement of physisorbed Li^+ by chemisorbed O_2^- when ORR starts, followed by the subsequent chemical reaction between adsorbed$O_2^-$with the solved Li^+ in the electrolyte or ii) to a direct reaction between the physisorbed Li^+ with the molecular O_2at the oxygen reduction potential to give Li_2O_2. Nevertheless, once the potential of ORR is surpassed (i.e. 2.2 V), the EDL capacitance increases again, what suggests that Li_2O_2 is not forming a monolayer on the top of the carbon surface. This idea is also supported by the study of C_{EDL} with the number of cycles, in which is observed that the same capacitance is obtained independently on the number of CV cycles, and then, on the formation of Li_2O_2 and Li_2CO_3. This result discards that the transport limitation and the cause of the low rechargeability of the current battery is the formation of an insulating layer (Li_2CO_3 or Li_2O_2) on the carbon porosity, as some authors have reported.[6, 22] Therefore, the transport blocking most probably become from the accumulation of these two species on one of the two sides of the electrode (electrode-electrolyte or electrode-O_2). Since the surface phenomena monitored by EIS (related to the electrode-electrolyte interface) are scarcely affected by the presence of these two species, one can infer that the accumulation of both, Li_2O_2 and Li_2CO_3, is at the electrode-O_2 interface, that finally limits the O_2 diffusion.[23] Noticeably EDLC remains unaltered after cycling. This fact suggests that the ORR products (Li_2O_2 and Li_2CO_3) are not covering the internal electrode surface, but deposited on the outer electrode-O_2 interface, hindering thereby the subsequent reaction.

In all the models for Li-O_2 discharge mechanism, the surface of the cathode is considered as a raw graphitic layer where the Li^+ ions arrive from the electrolyte side. This study demonstrates that the surface is already covered by adsorbed Li^+ when ORR starts what could imply that once the soluble O_2 react with Li^+, the molecular O_2can first react with the adsorbed Li^+ on the surface nearly the O_2, forming Li_2O_2 and avoiding further reaction. Qu et al. [11] reported that the discharge capacitance can be increased with O_2 pressure higher than 1 atm since the electrolyte was forced back from the interface and the complete wetting of the cathode is avoided. Therefore, adsorbed Li^+ consumption provides a new context of the cathode surface where the oxygen reduction reaction develops.

2.5. ORR Capacitance

At low voltages the reduction reaction of O_2 takes place. ORR is the main process in Li-O_2 batteries that provides the unique high capacity, but the main drawback for following this reaction by EIS is its extremely slow rate; it is registered at frequencies below 10 mHz. For this reason, the fitting of the data is only partial. In Figure 4b has been represented by a resistance in series with the chemical capacitance for the purpose of clarity. Nevertheless, in the Nyquist plot is observed that the real part of the impedance (-Z') increases, then signaling an extra resistive behavior in addition to the capacitive one observed in Figure 4a. For this reason, more elements than the chemical capacitance are certainly needed. It is indeed the final limiting step related to the O_2 diffusion through different layers. It is obvious that it is necessary to fast up this process in order to make it fully observable by impedance methods.

3. Experimental

All the agents were purchased from Sigma Aldrich, and were used as received. The cathodes were prepared by painting a carbon/PVdF slurry onto a stainless steel mesh. The slurries were prepared by mixing carbon black/PVdF/catalyst (60:10:30 % wt) and the addition of 1-Methyl-2-pyrrolidone. All the cathodes were dryed in vacuum, at 110 ºC overnight.Mixed-metal oxides are proved to be good catalysts for both ORR and OER in Li-O_2 batteries.[24] In this study, a commercial nanopowder, nickel cobalt oxide, (of size lower than 150 nm, CAS 5859-45-0, Sigma-Aldrich) was observed to accelerate H_2O_2 oxidation(Figure SI.8) and, consequently, it is a good candidate as catalyst for Li-O2 batteries,[25] albeit no reference of its use has been found in the literature. Despite its study is out of the topic of this manuscript, we have seen that its main contribution is the reduction of the charge transfer resistance (Figure SI.9).

Cell assembly (Swagelok type)was carried out in a N_2 filled glovebox. This consists simple in clamping together a Li metal foil anode, an electrolyte-soaked separator, the electrolyte that is 1M hexafluorophosphate lithium salt ($LiPF_6$) dissolved in tetraethylene glycol dimethyl ether (TEGDME), the cathode under study and the stainless steel current collector. The cathode collector is a tube in which pure O_2 (>99.9999 to avoid contamination issues) flows, the pressure is maintained at 1 atm during all the experiment.

Electrochemical characterization was performed using a PGSTAT-30 potentiostat from Autolab equipped with an impedance module. The CV was carried out in the voltage window of 2-4.0V at 100 $\mu V\ s^{-1}$scan rate. After 3 CV scans, the EIS spectra were performed (every 200 mV) within this voltage range with an amplitude perturbation of 10 mV, and in the frequency range of 1 MHz to 1 mHz. The approximation to the different voltages of measurement was potentiostically controlled at 10 $\mu V \cdot s^{-1}$ to assure

the quasi-equilibrium state of the battery. Also, before each measurement the system was stabilized during 30 minutes. All the data are normalized to the carbon mass.

The cycled electrodes were characterized by means of X-ray powder diffraction (XDR) using Bruker AXS-D4 Endeavor Advance X-ray diffractometer using Cu□ radiation. X-ray photoelectron spectroscopy (XPS) was performed on Sage 150 de Specs with non-monochromatic radiation AlKα (1486.6 eV) to 20 mA and 13 kV, a constant pass energy 75 eV for global analysis and 30 eV for specific binding energy of each element analysis, and an area measuring 1x1 mm^2. The base pressure of XPS chamber was 7×10^{-9} hPa. XPS spectra were fitted with CasaXPS software, which models the Gauss-Lorentzian contributions, after background subtraction. Also, energy spectra were calibrated by setting the C 1s photoemission peak for sp^2-hybridized carbon to 284.8 eV. Samples were washed out by anhydrous dimethyl carbonate (DMC, Sigma-Aldrich) solvent several times, and dried in a vacuum chamber at 60 ºC for 2 h previous XRD and XPS measurements.[26]

4. Conclusions

This manuscript analyzes the discharge process of Li-O_2 batteries by impedance spectroscopy and provides a novel equivalent circuit model. In this model, different electrochemical processes during discharge mechanism are identified: i) interfacial phenomena, ii) extended electrochemical double layer capacitance (EDLC), and iii) ORR chemical capacitance. EDLC has been monitored in Li-O_2 batteries and it is observed to be independent of the presence of O_2 at voltages higher than those at which oxygen reduction reaction occurs. Noticeably EDLC is fully recovered after electrode charging, and remains unaltered after cycling. This fact suggests that the ORR products (Li_2O_2 and Li_2CO_3) are not covering the internal electrode surface, but deposited on the outer electrode-O_2interface, hindering thereby the subsequent reaction. At this moment, further research is necessary to elucidate if these adsorbed Li^+ at the internal electrode

double layer can directly react with the O_2 molecules at the voltage where ORR starts or they are merely displaced by the reduction of O_2 molecules. The novel equivalent circuit model and the consideration that Li^+ ions are already adsorbed on the carbon surface when ORR starts provide new tools in the study and design of Li-O_2 cathodes.

Acnknowlegments

We thank financial support from Generalitat Valenciana (ISIC/ 2012/008 Institute of Nanotechnologies for Clean Energies). The authors acknowledge Dr. Conchi Ania from National Institute of Carbon for providing PSCo and AG carbons and their characterization.

References

[1] P. G. Bruce, S. A. Freunberger, L. J. Hardwick, J.-M. Tarascon, *Nature materials* **2012**, *11*, 19-29.

[2] N. S. Choi, Z. Chen, S. A. Freunberger, X. Ji, Y. K. Sun, K. Amine, G. Yushin, L. F. Nazar, J. Cho, P. G. Bruce, *Angewandte Chemie International Edition* **2012**, *51*, 9994-10024.

[3] aZ. Peng, S. A. Freunberger, Y. Chen, P. G. Bruce, *Science* **2012**, *337*, 563-566; bH.-G. Jung, J. Hassoun, J.-B. Park, Y.-K. Sun, B. Scrosati, *Nature chemistry* **2012**, *4*, 579-585; cB. G. Kim, H.-J. Kim, S. Back, K. W. Nam, Y. Jung, Y.-K. Han, J. W. Choi, *Scientific reports* **2014**, *4*; dZ. L. Wang, D. Xu, J. J. Xu, L. L. Zhang, X. B. Zhang, *Advanced Functional Materials* **2012**, *22*, 3699-3705.

[4] Z. Peng, S. A. Freunberger, L. J. Hardwick, Y. Chen, V. Giordani, F. Bardé, P. Novák, D. Graham, J. M. Tarascon, P. G. Bruce, *Angewandte Chemie* **2011**, *123*, 6475-6479.

[5] R. Wen, M. Hong, H. R. Byon, *Journal of the American Chemical Society* **2013**, *135*, 10870-10876.

[6] B. McCloskey, A. Speidel, R. Scheffler, D. Miller, V. Viswanathan, J. Hummelshøj, J. Nørskov, A. Luntz, *The Journal of Physical Chemistry Letters* **2012**, *3*, 997-1001.

[7] B. Scrosati, K. M. Abraham, W. A. van Schalkwijk, J. Hassoun, *Lithium Batteries: Advanced Technologies and Applications*, Wiley, **2013**.

[8] C. O. Laoire, S. Mukerjee, K. Abraham, E. J. Plichta, M. A. Hendrickson, *The Journal of Physical Chemistry C* **2009**, *113*, 20127-20134.

[9] aM. D. Radin, D. J. Siegel, *Energy & Environmental Science* **2013**, *6*, 2370-2379; bC. O. Laoire, S. Mukerjee, K. Abraham, E. J. Plichta, M. A. Hendrickson, *The Journal of Physical Chemistry C* **2010**, *114*, 9178-9186; cM. Safari, B. D. Adams, L. F. Nazar, *The Journal of Physical Chemistry Letters* **2014**, *5*, 3486-3491; dB. Horstmann, B. Gallant, R. Mitchell, W. G. Bessler, Y. Shao-Horn, M. Z. Bazant, *The Journal of Physical Chemistry Letters* **2013**, *4*, 4217-4222; eJ.-J. Xu, Z.-L. Wang, D. Xu, L.-L. Zhang, X.-B. Zhang, *Nature communications* **2013**, *4*.

[10] aL. Johnson, C. Li, Z. Liu, Y. Chen, S. A. Freunberger, P. C. Ashok, B. B. Praveen, K. Dholakia, J.-M. Tarascon, P. G. Bruce, *Nature chemistry* **2014**, *6*, 1091-1099; bK.-H. Xue, E. McTurk, L. Johnson, P. G. Bruce, A. A. Franco, *Journal of The Electrochemical Society* **2015**, *162*, A614-A621.
[11] C. Tran, X.-Q. Yang, D. Qu, *Journal of power sources* **2010**, *195*, 2057-2063.
[12] J. Højberg, B. D. McCloskey, J. Hjelm, T. Vegge, K. Johansen, P. Norby, A. C. Luntz, *ACS applied materials & interfaces* **2015**, *7*, 4039-4047.
[13] aP. Simon, Y. Gogotsi, *Nature materials* **2008**, *7*, 845-854; bM. Haro, G. Rasines, C. Macias, C. Ania, *Carbon* **2011**, *49*, 3723-3730.
[14] aS. Y. Kim, H.-T. Lee, K.-B. Kim, *Physical Chemistry Chemical Physics* **2013**, *15*, 20262-20271; bF. Li, R. Ohnishi, Y. Yamada, J. Kubota, K. Domen, A. Yamada, H. Zhou, *Chem. Commun.* **2013**, *49*, 1175-1177.
[15] S. A. Freunberger, Y. Chen, N. E. Drewett, L. J. Hardwick, F. Bardé, P. G. Bruce, *Angewandte Chemie International Edition* **2011**, *50*, 8609-8613.
[16] M. M. Ottakam Thotiyl, S. A. Freunberger, Z. Peng, P. G. Bruce, *Journal of the American Chemical Society* **2012**, *135*, 494-500.
[17] F. Martinez-Julian, A. Guerrero, M. Haro, J. Bisquert, D. Bresser, E. Paillard, S. Passerini, G. Garcia-Belmonte, *The Journal of Physical Chemistry C* **2014**, *118*, 6069-6076.
[18] M. Haro, T. Song, A. Guerrero, L. Bertoluzzi, J. Bisquert, U. Paik, G. Garcia-Belmonte, *Physical Chemistry Chemical Physics* **2014**, *16*, 17930-17935.
[19] W.-C. Chen, T.-C. Wen, *Journal of power sources* **2003**, *117*, 273-282.
[20] C. Vix-Guterl, S. Saadallah, K. Jurewicz, E. Frackowiak, M. Reda, J. Parmentier, J. Patarin, F. Beguin, *Materials Science and Engineering: B* **2004**, *108*, 148-155.
[21] F. Béguin, E. Frackowiak, *Carbons for electrochemical energy storage and conversion systems*, CRC Press, **2009**.
[22] P. Albertus, G. Girishkumar, B. McCloskey, R. S. Sánchez-Carrera, B. Kozinsky, J. Christensen, A. Luntz, *Journal of The Electrochemical Society* **2011**, *158*, A343-A351.
[23] S. Sandhu, J. Fellner, G. Brutchen, *Journal of power sources* **2007**, *164*, 365-371.
[24] aJ.-J. Xu, Z.-L. Wang, D. Xu, F.-Z. Meng, X.-B. Zhang, *Energy & Environmental Science* **2014**, *7*, 2213-2219; bJ. J. Xu, D. Xu, Z. L. Wang, H. G. Wang, L. L. Zhang, X. B. Zhang, *Angewandte Chemie International Edition* **2013**, *52*, 3887-3890.
[25] V. Giordani, S. Freunberger, P. Bruce, J.-M. Tarascon, D. Larcher, *Electrochemical and Solid-State Letters* **2010**, *13*, A180-A183.
[26] M. H. Rui Wen, and Hye Ryung Byon, *Journal of the American Chemical Society* **2013**, *135*, 10870 - 10876.

Figure Captions

Figure 1. (a) CV of SP@30NiOCoO in the presence of O_2 along different number of cycles and in the absence of O_2 (inset). Scan rate: 0.1 mV s^{-1}. (b) XRD patters of air cathode before being cycled and after 3 and 7 cycles. The patters of the pristine mesh, Li_2O_2, NiO·CoO, and Li_2CO_3 are also shown.

Figure 2. Nyquist plots of SP@30% NiOCoO with and without O_2.The low frequency (< 5 Hz) region of the EIS is observed in graphs a-c, and the figures d-f show an

enlargement of the high frequency region. The experimental data are represented by solid symbols and the lines are obtained by the fitting with the equivalent circuit model shown in Figure 4 b.

Figure 3. Capacitance plot of SP@30% NiOCoO with and without O_2. The experimental data are represented by solid symbols and the lines are obtained by the fitting with the equivalent circuit model shown in Figure 4.b.

Figure 4. (a) C' vs characteristic time and frequency (in opposite order than usual, from fast to slow electrochemical processes for a more intuitive reading) for SP@30NiOCoO in the presence (solid lines) and absence (dashed lines) of O_2. Inset: Scheme of the three processes of the Li-O_2 discharge mechanism. The ORR is represented on the cathode surface by a graphitic layer, in which adsorbed Li^+ react with O_2. (b) Equivalent circuit model for the system in the absence and presence of O_2.

Figure 5. Parameters determined during discharge process by the EIS fitting with the equivalent circuit model shown in Figure 4.b: (a) resistance and (b) capacitance associated to the interface phenomena;(c) resistance, R_{ads}, and (d) capacitance, C_{EDL}, associated to the formation of the electrochemical double layer; (e) parallel resistance, R_{ORR}, which decrease at the applied voltages when the ORR starts.

Figure 6. (a) Nyquist and (b) EDL capacitance plots of the SP@30% NiOCoO air cathode at 3.4 V at different number of CV cycles.

Adsorbed Li^+ consumption is monitored during oxygen reduction reaction (ORR) providing further understanding on the discharge process of Li-O_2 batteries. Adsorbed Li^+ is inferred from extended electrochemical double layer capacitance (EDLC), which is function on the carbon matrix surface area. EDLC is independent of the presence of Li_2O_2 and Li_2CO_3, what indicates that the precipitation occurs at the electrode-O_2 interface and not inside the electrode porosity.

Keyword

Li-O_2Batteries, Adsorption, Impedance Spectroscopy, Electrochemical Double Layer

Marta Haro*, Nuria Vicente, GermàGarcia-Belmonte*

Oxygen Reduction Reaction Promotes Li^+ Desorption from Cathode Surface in Li-O_2 Batteries